



## INTERFACE STABILITY UNDER BIAXIAL LOADING OF BILAYERED SHEETS BETWEEN RIGID SURFACES—I. BIFURCATION ANALYSIS

J. L. ALCARAZ.

Departamento de Ingeniería Mecánica-Escuela Técnica Superior de Ingenieros,  
Alameda Urquijo, s/n-48013 Bilbao, Spain

J. M. MARTÍNEZ-ESNAOLA and J. GIL-SEVILLANO

Centro de Estudios e Investigaciones Técnicas de Guipúzcoa (CEIT) and Escuela Superior de  
Ingenieros Industriales (Universidad de Navarra)-P<sup>o</sup> Manuel de Lardizábal,  
15-20009 San Sebastián, Spain

(Received 23 March 1995)

**Abstract** A bifurcation method has been applied to the plastic stability analysis of a bimetallic sheet between rigid surfaces subjected to biaxial loading. An orthotropic, incrementally-linear solid and plane strain conditions are assumed. In order to predict the stability behaviour near the bimaterial interface, three possible regimes (elliptic, hyperbolic and parabolic) are considered and two modes of instability are mentioned, namely: the diffuse mode, characterized by spatially periodic deformations, and the localized shear band mode. In general, undulations can be expected in the elliptic regime and shear band instabilities only appear in the hyperbolic and parabolic regimes. Attention is concentrated on the diffuse mode. Critical equivalent strains have been obtained, as a function of a wavenumber defined in the analysis. Numerical results are presented for three different constitutive models and for a number of combinations of the geometric and material parameters, to assess their influence on the critical strain. Copyright © 1996 Elsevier Science Ltd.

### 1. INTRODUCTION

Much effort is currently devoted to the design and processing of bimaterial products because of their potential ability to combine physical and chemical properties of different materials. This is a very attractive feature in specific industrial technology. For instance, consider the use of bimetallic structures in applications where it is desired to combine a high mechanical strength and a good protection against oxidation and corrosion.

One problem encountered in some metal forming processes of bimaterial layers is the appearance of thickness fluctuations and occasional decohesion along the interface, basically due to the material heterogeneity and high strains during those processes. The analysis of this phenomenon, under the point of view of bifurcation and plastic stability, has motivated the present paper.

Stability of plastic solids has become a relevant research topic in the fields of plasticity and metalworking. In the case of a single material, Hill and Hutchinson (1975) and Young (1976) investigated the bifurcation phenomenon in an homogeneous incompressible rectangular block subjected to uniaxial stress under plane strain conditions. Later, Hutchinson and Tvergaard (1980) considered the existence of surface instabilities in a semi-infinite solid with free boundaries by using either a bifurcation analysis or a quasi-static, imperfection-growth analysis. A strong dependence on the type of constitutive law assumed was found. These analyses show that instabilities are predicted when a finite strain deformation theory is assumed. More recently, Dudzinski and Molinari (1991) have analysed the thermoviscoplastic instabilities in a material subjected to biaxial loading by using a perturbation method, which is proposed as an alternative to the bifurcation method. In this analysis, the rate of growth of infinitesimal perturbations is obtained for quite general material behaviours.

The analysis is more complex in the bimaterial case. Steif (1986b) has considered the periodic necking instabilities of a solid composed of alternating material layers under uniaxial

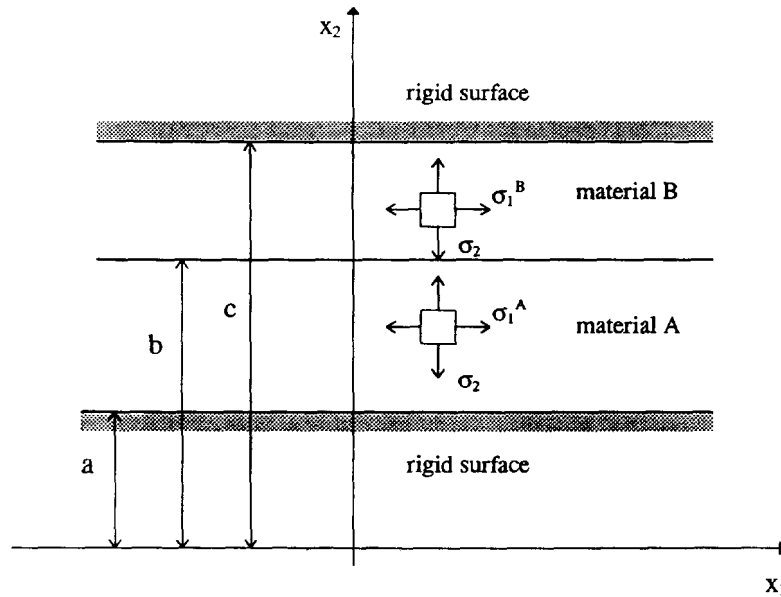


Fig. 1. Geometry of the problem.

tension. Conditions for periodic incremental deformations, consistent with an overall homogeneous stretching, are obtained. The competition of the undulatory modes with shear localization is also examined. More recently, Tomita and Kim (1992) have considered the non-axisymmetric bifurcation behaviour of bilayered tubes subjected to uniform shrinkage at the external surface in plane strain. It is concluded that the yield stress ratio and the hardening exponent ratio substantially affect the bifurcation mode with long wavelength. Independently, Suo *et al.* (1992) have investigated the stability for two semi-infinite solids bonded with a planar interface. A traction-displacement jump relation characterizes the interface, so that dimensional considerations introduce a characteristic length. Stability is analysed, with the aid of complex variable methods, in terms of the existence of certain stationary waves.

In this paper, we are concerned with the instability analysis of a bimaterial layer placed between rigid surfaces and subjected to biaxial loading. The existence of non-uniform solutions is investigated by using a bifurcation method. This method is similar, to some extent, to that of Steif (1986b) in uniaxial tension; but here we proceed with other boundary conditions and biaxial stress states, and furthermore, a different resolution procedure and a more complete analysis are presented. The bifurcation equation for the problem is established and solved numerically to obtain a critical strain in terms of a characteristic wavenumber, for different values of the geometric and material parameters of the process. The influence of the relevant parameters on the bifurcation behaviour is discussed.

Three different constitutive models are considered in the calculations (the so named Voce, Prager and Hollomon models). In the bibliography, attention is given especially to the last one, the Hollomon model, which is not adequate to describe the actual material behaviour at high plastic strains, especially at high temperatures. The two other models seem, however, more appropriate under such conditions.

It should be noted that this study could be applied, as a first approximation, to different metal forming processes involving a bimaterial composite under a biaxial stress state.

## 2. GOVERNING EQUATIONS

Consider a plane bilayer consisting of two materials with finite thickness and infinite length: *A* (between  $x_2 = a$  and  $x_2 = b$ ) and *B* (between  $x_2 = b$  and  $x_2 = c$ ), the set being limited by two rigid surfaces fixed at  $x_2 = a$  and  $x_2 = c$ , as shown schematically in Fig. 1.

Incompressibility, plane strain conditions, as well as time independent behaviour, are considered in the model. Assume that the deformation up to a certain instant is homogeneous,

with principal axes  $x_1$  and  $x_2$ , and that both materials,  $A$  and  $B$ , are orthotropic along these axes.

Assuming that the hydrostatic pressure does not influence the constitutive relation between the deviators of stress rate and strain rate, the constitutive law for incrementally linear solids necessarily has the following structure (Biot, 1965):

$$\begin{aligned}\dot{\hat{\sigma}}_{11} - \dot{\hat{\sigma}}_{22} &= 2\mu^*(\dot{e}_{11} - \dot{e}_{22}) \\ \dot{\hat{\sigma}}_{12} &= 2\mu w_{12}, \quad \dot{\hat{\sigma}}_{21} = \dot{\hat{\sigma}}_{12}\end{aligned}\quad (1)$$

where  $\dot{\hat{\sigma}}_{ij}$  is the Jaumann derivative (referred to the rotating axes) of the true stress;  $e_{ij}$  is the eulerian strain rate,  $e_{ij} = (v_{i,j} + v_{j,i})/2$ ,  $v_i$  being the velocity and  $(\cdot)_{,i}$  denoting partial differentiation with respect to  $x_i$ ;  $\mu$  and  $\mu^*$  are two incremental shear moduli. At the moment of the analysis, the stress components are  $\sigma_{11} = \sigma_1$  and  $\sigma_{22} = \sigma_2$ . It is assumed that the current stress components are uniform in each material. As shown in Fig. 1,  $\sigma_1$  can be different in  $A$  and  $B$ .

It is convenient to express (1) in terms of nominal stress rates  $\dot{n}_{ij}$ , which are related to Jaumann derivatives and true stresses through the expression:

$$\dot{n}_{ij} = \dot{\hat{\sigma}}_{ij} + \sigma_{ik} w_{jk} + \sigma_{jk} w_{ik} - \sigma_{jk} \frac{\partial v_i}{\partial x_k} \quad (2)$$

where  $w_{ij}$  is the spin tensor,  $w_{ij} = (v_{i,j} - v_{j,i})/2$ , and the convention of summing over repeated indices is applied.

By using the incompressibility condition ( $v_{i,i} = 0$ ) and introducing a flow function  $\psi(x_1, x_2)$  so that  $v_1 = \partial\psi/\partial x_2$ ,  $v_2 = -\partial\psi/\partial x_1$ , the equilibrium equations  $\dot{n}_{i,j} = 0$  lead to the following partial derivative equation:

$$\left(\mu + \frac{1}{2}(\sigma_1 - \sigma_2)\right) \frac{\partial^4 \psi}{\partial x_1^4} + 2(2\mu^* - \mu) \frac{\partial^4 \psi}{\partial x_1^2 \partial x_2^2} + \left(\mu - \frac{1}{2}(\sigma_1 - \sigma_2)\right) \frac{\partial^4 \psi}{\partial x_2^4} = 0 \quad (3)$$

This equation can also be obtained as a particular case of a more general equation deduced in Appendix A.

On the other hand, the continuity conditions at the interface are:

$$\left. \begin{aligned}v_2^A &= v_2^B \\ v_1^A &= v_1^B \\ \dot{n}_{22,1}^A &= \dot{n}_{22,1}^B \\ \dot{n}_{21}^A &= \dot{n}_{21}^B\end{aligned} \right\} \text{ at } x_2 = h \quad (4)$$

where the third equation replaces, for convenience, the continuity condition of the normal component of the nominal stress rate.

Equations (4) can be rewritten in terms of  $\psi$  as:

$$\begin{aligned}\left\langle \frac{\partial \psi}{\partial x_1} \right\rangle &= \left\langle \frac{\partial \psi}{\partial x_2} \right\rangle = 0 \\ \left\langle \left(4\mu^* - \mu - \frac{\sigma_1 + \sigma_2}{2}\right) \frac{\partial^3 \psi}{\partial x_1^2 \partial x_2} + \left(\mu - \frac{\sigma_1 - \sigma_2}{2}\right) \frac{\partial^3 \psi}{\partial x_2^3} \right\rangle &= 0 \\ \left\langle -\left(\mu - \frac{\sigma_1 + \sigma_2}{2}\right) \frac{\partial^2 \psi}{\partial x_1^2} + \left(\mu - \frac{\sigma_1 - \sigma_2}{2}\right) \frac{\partial^2 \psi}{\partial x_2^2} \right\rangle &= 0\end{aligned}\quad (5)$$

where the sign  $\langle \rangle$  indicates the change in the enclosed magnitude on crossing the interface at  $x_2 = b$ .

Finally, the boundary conditions are expressed as:

$$\begin{aligned} v_2^A &= 0 \quad \text{at} \quad x_2 = a \\ v_2^B &= 0 \quad \text{at} \quad x_2 = c \end{aligned} \quad (6)$$

and in terms of  $\psi$ :

$$\left. \frac{\partial \psi_A}{\partial x_1} \right|_{x_2=a} = 0; \quad \left. \frac{\partial \psi_B}{\partial x_1} \right|_{x_2=c} = 0. \quad (7)$$

Equation (3) is more shortly written as:

$$(R+S) \frac{\partial^4 \psi}{\partial x_1^4} + 2(1-R) \frac{\partial^4 \psi}{\partial x_1^2 \partial x_2^2} + (R-S) \frac{\partial^4 \psi}{\partial x_2^4} = 0, \quad (8)$$

with the following notation:

$$R = \frac{\mu}{2\mu^*}, \quad S = \frac{\sigma_1 - \sigma_2}{4\mu^*} \quad (9)$$

### 3. EIGENMODES AND BIFURCATION EQUATION

Suppose that an increment in the far field displacements is applied at a given instant. We confine attention to analysing whether a non uniform solution is possible. In particular, let us seek for periodical solutions at the neighbourhood of the interface in a separate variable form, as follows:

$$\psi = f(x_2) \sin \frac{2\pi x_1}{\lambda} \quad (10)$$

where  $\lambda$  is the wavelength of the deformation in the  $x_1$  direction and  $f(x_2)$  has to be selected so that  $v_1$  and  $v_2$  verify the continuity conditions.

When (10) is introduced in (8), a fourth-order differential equation is found for the function  $f$ , whose characteristic equation has the following roots:

$$z^2 = \frac{(R-1) \pm \sqrt{(R-1)^2 - (R^2 - S^2)}}{R-S}. \quad (11)$$

There will be, in general, two distinct roots for  $z^2$ , the character of the solution depending on whether the roots are real or not. Following the classical notation used in this field, the regime is said to be elliptic (*E*), hyperbolic (*H*) or parabolic (*P*) according to whether there are zero, four or two real roots, respectively, for the characteristic equation. Some comments on the meaning of the characteristics of (8) are included in Appendix B. In view of (10), the three regimes are determined by:

$$(E) \text{ zero real roots: } R > (1+S^2)/2 \quad \text{or} \quad (1+S^2)/2 > R > S \quad \text{and} \quad R < 1 \quad (12a)$$

$$(H) \text{ four real roots: } S < R < (1+S^2)/2 \quad \text{and} \quad R > 1 \quad (12b)$$

$$(P) \text{ two real roots: } S > R \quad (12c)$$

Not all the values of  $R$  and  $S$  are possible. As demonstrated by Hill and Hutchinson

(1975), there is a condition excluding the possibility of first-order bifurcation for incrementally linear materials. This condition is associated with the principle that the loads do less work than expended internally, and leads to the relations:

$$0 < \sigma_1 + \sigma_2 < 4\mu^* \quad \text{and} \quad \frac{\sigma_1^2 + \sigma_2^2}{\sigma_1 + \sigma_2} < 2\mu \tag{13}$$

In terms of  $R$  and  $S$  (for positive  $R$  and  $S$ ):

$$R > \frac{\sigma_1^2 + \sigma_2^2}{\sigma_1 - \sigma_2} S \equiv aS \quad \text{and} \quad S < \frac{\sigma_1 - \sigma_2}{\sigma_1 + \sigma_2} \equiv b \tag{14}$$

If  $\sigma_1 > \sigma_2 > 0$ , then  $a > 1$  and  $b < 1$ . For this case, Fig. 2 shows the different regions and boundaries in the space  $R-S$  ( $R > 0, S > 0$ ). Note that the elliptic zone contacts the hyperbolic region (for  $S > 1$ ) as well as the parabolic region (for  $0 < S < 1$ ).

3.1. *Elliptic regime in A and B*

According to (12a), there will be no real roots in  $A$  and  $B$  when  $R > (1+S^2)/2$  or both  $(1+S^2)/2 > R > S$  and  $R < 1$  are satisfied in each material. The functions  $f_A$  and  $f_B$  which make the boundary conditions (7) be verified can be expressed for a symmetric mode and  $x_2 > 0$ —as:

$$f_A(x_2) = \Re \left\{ h_1 \cdot \sin \frac{2\pi}{\lambda} x(x_2 - a) \right\} \tag{15a}$$

$$f_B(x_2) = \Re \left\{ h_2 \cdot \sin \frac{2\pi}{\lambda} \beta(c - x_2) \right\} \tag{15b}$$

where  $\Re$  denotes the real part of the enclosed quantity,  $h_1$  and  $h_2$  are complex constants, and, according to (11),

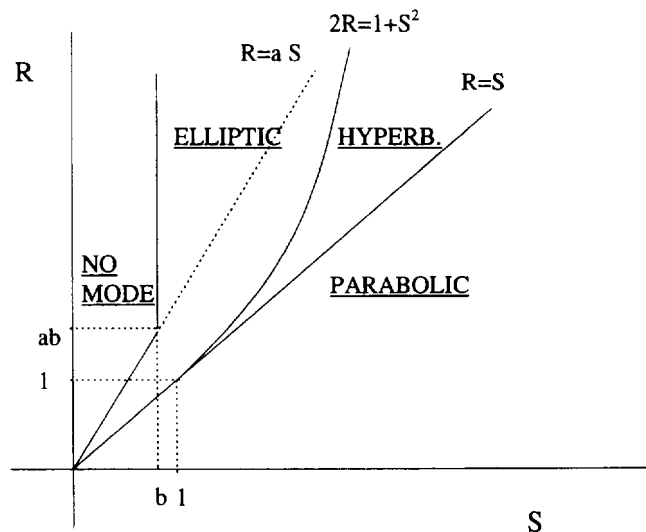


Fig. 2. A representation of the characteristic regimes.

$$x^2 = \frac{R_A - 1 \pm \sqrt{S_A^2 - 2R_A + 1}}{R_A - S_A} \quad (16a)$$

$$\beta^2 = \frac{R_B - 1 \pm \sqrt{S_B^2 - 2R_B + 1}}{R_B - S_B} \quad (16b)$$

By imposing the continuity conditions (5) at the interface and after doing some algebra, the following homogeneous system is obtained

$$\begin{aligned} \Re\{h_1 \cdot \sin q_A x - h_2 \cdot \sin q_B \beta\} &= 0 \\ \Re\{h_1 \cdot x \cdot \cos q_A x + h_2 \cdot \beta \cdot \cos q_B \beta\} &= 0 \\ \Re\{h_1 [(R_A - S_A)x^2 - (R_A + S_A - 2)]x \cos q_A x + \xi h_2 [(R_B - S_B)\beta^2 - (R_B + S_B - 2)]\beta \cos q_B \beta\} &= 0 \\ \Re\{h_1 [x^2(R_A - S_A) - (R_A - S_A)] \sin q_A x - \xi h_2 [\beta^2(R_B - S_B) - (R_B - S_B)] \sin q_B \beta\} &= 0 \end{aligned} \quad (17)$$

where

$$S = \frac{\sigma_1 + \sigma_2}{4\mu^*}, \quad q_A = \frac{2\pi}{\lambda}(h-a), \quad q_B = \frac{2\pi}{\lambda}(c-b), \quad \xi = \frac{\mu_B^*}{\mu_A^*} \quad (18)$$

The resolution procedure of the equation system (17) is as follows: from the first two equations of (17), we express the real and imaginary parts of  $h_2$  in terms of those of  $h_1$ ; then they are inserted in the last two equations of (17) and  $h_1$  is eliminated. After lengthy manipulations and denoting  $x = p_A + ir_A$ ,  $\beta = p_B + ir_B$ , the following bifurcation equation is deduced:

$$\begin{aligned} (R_A - S_A) &\left\{ \frac{S_A^I}{p_A} [X_A(1 - S_A) - S_A^I] + \frac{S_A^I}{r_A} [X_A(1 - S_A) + S_A^I] \right\} \left[ \frac{S_B^B}{p_B} - \frac{S_B^B}{r_B} \right] \\ &+ \xi^2 \left[ \frac{S_A^I}{p_A} - \frac{S_A^I}{r_A} \right] (R_B - S_B) \left\{ \frac{S_B^B}{p_B} [X_B(1 - S_B) - S_B^B] + \frac{S_B^B}{r_B} [X_B(1 - S_B) + S_B^B] \right\} \\ &- \xi \left\{ 2(R_A - S_A)(R_B - S_B) [X_A(c_p^I + c_r^I)(c_r^B - c_p^B) + X_B(c_r^I - c_p^I)(c_r^B + c_p^B)] \right. \\ &+ 2(1 - S_A)(R_B - S_B) \left[ \frac{S_p^I}{p_A} - \frac{S_r^I}{r_A} \right] (p_B s_p^B + r_B s_r^B) + (1 - S_A)(1 - S_B) \left[ \frac{S_p^I}{p_A} - \frac{S_r^I}{r_A} \right] \left[ \frac{S_B^B}{p_B} - \frac{S_B^B}{r_B} \right] \\ &+ 4(R_A - S_A)(R_B - S_B)(p_A s_p^I + r_A s_r^I)(p_B s_p^B + r_B s_r^B) \\ &\left. + 2(1 - S_B)(R_A - S_A) \left[ \frac{S_p^B}{p_B} - \frac{S_r^B}{r_B} \right] (p_A s_p^I + r_A s_r^I) \right\} = 0 \end{aligned} \quad (19)$$

where, to be concise, the following notation has been used:

$$s_p = \sin 2pq, \quad c_p = \cos 2pq, \quad s_r = \sinh 2rq, \quad c_r = \cosh 2rq \quad (20a)$$

$$X = \sqrt{(R+S)(R-S)} \quad (20b)$$

$$S^I = \left( RS - \frac{S^2 + S'^2}{2} \right) (R-S) \quad (20c)$$

and  $p_A, r_A$  are given by

$$p_A^2 = \frac{2R_A + S_A - 1}{2(R_A - S_A)}; \quad r_A^2 = \frac{S_A + 1}{2(R_A - S_A)} \quad (20d)$$

3.1.1. *Particular cases.* Consider now two particular cases: (a) a monomaterial case and (b) a bimaterial case under uniaxial state. Since these cases are reported in other related papers mentioned in Section 1, they will be used to check the consistency of all the results along this section.

(a) Monomaterial case

Suppose that  $\xi \rightarrow 0$  (i.e.,  $\mu_B^* = 0$  or  $\mu_A^* \rightarrow \infty$ ). This situation is equivalent to the case of only material  $A$  existing. Then (19) reduces to

$$\frac{r_A \sin 2q_A p_A}{p_A \sinh 2q_A r_A} = \frac{S_A + X_A(1 - S_A)}{S_A - X_A(1 - S_A)} \quad (21)$$

Moreover, in a uniaxial problem, (21) changes into:

$$\frac{r_A \sin 2q_A p_A}{p_A \sinh 2q_A r_A} = \frac{S_A + X_A(1 - S_A)}{S_A - X_A(1 - S_A)} \quad (22)$$

which coincides with the result obtained by Hill and Hutchinson (1975) for a single rectangular material under tension.

Similarly, in the case  $\xi \rightarrow \infty$  ( $\mu_A^* = 0$  or  $\mu_B^* \rightarrow \infty$ ), as if only material  $B$  is present, we obtain:

$$\frac{r_B \sin 2q_B p_B}{p_B \sinh 2q_B r_B} = \frac{S_B + X_B(1 - S_B)}{S_B - X_B(1 - S_B)} \quad (23)$$

which is exactly (21) by replacing  $A$  by  $B$ .

(b) Uniaxial state

If one of the biaxial stress components is negligible (for example,  $\sigma_2 \ll \sigma_1$ ), then:  $S' \approx S \approx \sigma_1 / 4\mu^*$ ;  $S'' \approx S$ , and (19) reduces to the solution presented by Steif (1986b).

### 3.2. Hyperbolic regime in $A$ and elliptic in $B$

Let us now analyze the case of  $A$  being in the hyperbolic regime ( $B$  remaining elliptic). Then, according to (12b), there will be four real roots in  $A$  when the conditions

$$\frac{1 + S_A^2}{2} > R_A > S_A \quad \text{and} \quad R_A > 1 \quad (24)$$

are fulfilled. The appropriate function  $f_A$  is now written –also for a symmetric mode– as:

$$f_A(x_2) = c_1 \cdot \sin \frac{2\pi}{\lambda} p_A(x_2 - a) + c_2 \cdot \sin \frac{2\pi}{\lambda} r_A(x_2 - a) \quad (25)$$

where  $c_1$  and  $c_2$  are real constants, and  $p_A^2 > 0$  and  $r_A^2 > 0$  are the solutions for  $\alpha^2$  (see (16a)). The function  $f_B$  is given by (15b),  $\beta^2$  remaining complex in the form  $\beta^2 = p_B + ir_B$  (see (16b)). It can also be checked that the function  $\psi_A$  obtained from  $f_A$  satisfies the first boundary condition in (7).

The continuity conditions at the interface (5) lead to:

$$\begin{aligned} c_1 \cdot \sin p_A q_A + c_2 \cdot \sin r_A q_A &= \Re\{h_2 \cdot \sin q_B \beta\} \\ c_1 \cdot p_A \cdot \cos p_A q_A + c_2 \cdot r_A \cos r_A q_A &= \Re\{-h_2 \cdot \beta \cdot \cos q_B \beta\} \\ (2 - R_A - S_A)(c_1 \cdot p_A \cdot \cos p_A q_A + c_2 \cdot r_A \cos r_A q_A) & \end{aligned}$$

$$\begin{aligned}
& + (R_A - S_A)(c_1 \cdot p_A^3 \cdot \cos p_A q_A + c_2 \cdot r_A^3 \cos r_A q_A) = \zeta[(2 - R_B - S'_B)\Re\{-h_2 \cdot \beta \cdot \cos q_B \beta\}] \\
& + (R_B - S_B)\Re\{-h_2 \cdot \beta^3 \cdot \cos q_B \beta\}] \\
& (R_A - S_A)(c_1 \cdot p_A^2 \sin p_A q_A + c_2 \cdot r_A^2 \sin r_A q_A) - (R_A - S'_A)(c_1 \cdot \sin p_A q_A + c_2 \cdot \sin r_A q_A) \\
& = \zeta[(R_B - S_B)\Re\{h_2 \cdot \beta^2 \cdot \sin q_B \beta\} - (R_B - S'_B)\Re\{h_2 \cdot \sin q_B \beta\}]. \quad (26)
\end{aligned}$$

By expanding the  $\Re$  terms in (26) and eliminating the constants  $c_1$  and  $c_2$ , the following bifurcation equation can be obtained:

$$\begin{aligned}
& (R_A - S_A)^2[(\kappa - p_A^2)^2 W_r^A Q_p^A - (\kappa - r_A^2)^2 W_p^A Q_r^A][r_B s_p^B - p_B s_r^B] \\
& - 2\zeta(R_A - S_A)(R_B - S_B)\{[(\kappa - p_A^2)W_r^A Q_p^A - (\kappa - r_A^2)W_p^A Q_r^A][r_B(1 + X_B)s_p^B \\
& + p_B(X_B - 1)s_r^B] - p_B r_B(p_A^2 - r_A^2)[W_p^A W_r^A(c_r^B - c_p^B) + X_B Q_r^A Q_p^A(c_r^B + c_p^B)]\} \\
& + 2\zeta^2(R_B - S_B)[W_r^A Q_p^A - W_p^A Q_r^A]\{r_B[(1 - S'_B)X_B - S_B]s_p^B + p_B[(1 - S'_B)X_B + S_B]s_r^B\} = 0
\end{aligned} \quad (27)$$

where the new notation is:

$$\begin{aligned}
\kappa &= \frac{R_A - S'_A}{R_A - S_A} \\
Q_p &= \sin pq, \quad Q_r = \sin rq, \quad W_p = p \cos pq, \quad W_r = r \cos rq.
\end{aligned} \quad (28)$$

### 3.2.1. Particular cases. (a) Monomaterial case

If  $\zeta \rightarrow 0$  (i.e., only material  $A$  is present), we obtain the following solution:

$$\frac{r_A \tan p_A q_A}{p_A \tan r_A q_A} = \left( \frac{\kappa_A - r_A^2}{\kappa_A - p_A^2} \right)^2 \quad (29)$$

Now, if the stress state is uniaxial, then  $\kappa_A = 1$  and we recover the solution by Hill and Hutchinson (1975) for the tension test of a rectangular material.

Likewise, if  $\zeta \rightarrow \infty$  (only  $B$ ), we attain to the same expression given by (23).

### (b) Uniaxial state

For the uniaxial stress case, the solution can be obtained by setting  $\kappa = 1$  (in  $A$ ) and  $S' = S'' = S$  (in  $B$ ), and coincides with that of Steif (1986b).<sup>†</sup>

### 3.3. Hyperbolic regime in A and B

Now consider the situation where both materials are in the hyperbolic regime. Then relations (12b) hold in  $A$  and  $B$ .

The functions  $f_A$  and  $f_B$  are now given by:

$$\begin{aligned}
f_A(x_2) &= c_1 \cdot \sin \frac{2\pi}{\lambda} p_A(x_2 - a) + c_2 \cdot \sin \frac{2\pi}{\lambda} r_A(x_2 - a) \\
f_B(x_2) &= d_1 \cdot \sin \frac{2\pi}{\lambda} p_B(c - x_2) + d_2 \cdot \sin \frac{2\pi}{\lambda} r_B(c - x_2)
\end{aligned} \quad (30)$$

where  $p_A^2$  and  $r_A^2$  are the solutions for  $x^2$ ;  $p_B^2$  and  $r_B^2$  are the solutions for  $\beta^2$  (see (16a,b)), and  $c_1, c_2, d_1, d_2 \in \Re$ . It is easy to check that the corresponding  $\psi$  functions verify the boundary conditions (7).

The interface conditions lead to:

<sup>†</sup> An error in Steif (1986b) [eqn for case (iii) in Appendix] has been detected: on the second line,  $(1 - p_A^2)^2$  and  $(1 - r_A^2)^2$  should not be squared and read as  $(1 - p_A^2)$  and  $(1 - r_A^2)$ .

$$\begin{aligned}
c_1 Q_p^A + c_2 Q_r^A - d_1 Q_p^B - d_2 Q_r^B &= 0 \\
c_1 W_p^A + c_2 W_r^A + d_1 W_p^B + d_2 W_r^B &= 0 \\
(w_A + \theta_A) c_1 W_p^A + (w_A - \theta_A) c_2 W_r^A + \zeta(w_B + \theta_B) d_1 W_p^B + \zeta(w_B - \theta_B) d_2 W_r^B &= 0 \\
(w_A - \theta_A) c_1 Q_p^A + (w_A + \theta_A) c_2 Q_r^A - \zeta(w_B - \theta_B) d_1 Q_p^B - \zeta(w_B + \theta_B) d_2 Q_r^B &= 0
\end{aligned} \quad (31)$$

where  $Q_p$ ,  $Q_r$ ,  $W_p$  and  $W_r$  are again given by (28) and

$$\begin{aligned}
w &= 1 - S \\
\theta &= \sqrt{S^2 - 2R + 1}.
\end{aligned} \quad (32)$$

The elimination of the constants  $c_1$ ,  $c_2$ ,  $d_1$  and  $d_2$  can be accomplished by imposing the vanishing of the determinant of the system. After several manipulations, the following bifurcation equation is achieved:

$$\begin{aligned}
(R_A - S_A)^2 &[(\kappa_A - p_A^2)^2 W_p^A Q_p^A - (\kappa_A - r_A^2)^2 Q_r^A W_p^A](Q_r^B W_p^B - Q_p^B W_r^B) + \zeta^2 (R_B - S_B)^2 \\
&\times [(\kappa_B - p_B^2)^2 W_r^B Q_p^B - (\kappa_B - r_B^2)^2 Q_r^B W_p^B](Q_r^A W_p^A - Q_p^A W_r^A) + 2\zeta (R_A - S_A)(R_B - S_B) \\
&\times [(\kappa_A - p_A^2)(\kappa_B - p_B^2) Q_p^A Q_p^B W_r^A W_r^B + (\kappa_A - r_A^2)(\kappa_B - r_B^2) Q_r^A Q_r^B W_p^A W_p^B \\
&- (\kappa_A - p_A^2)(\kappa_B - r_B^2) Q_p^A Q_r^B W_r^A W_p^B - (\kappa_A - r_A^2)(\kappa_B - p_B^2) Q_r^A Q_p^B W_p^A W_r^B \\
&+ \frac{1}{2}(p_A^2 - r_A^2)(p_B^2 - r_B^2)(Q_p^A Q_r^A W_r^B W_p^B + Q_r^B Q_p^B W_r^A W_p^A)] = 0.
\end{aligned} \quad (33)$$

### 3.3.1. Particular cases. (a) Monomaterial case

For  $\zeta \rightarrow 0$  (only material  $A$ ), (33) turns into (29). And for  $\zeta \rightarrow \infty$  (only  $B$ ), the resultant expression is:

$$\frac{r_B \tan p_B q_B}{p_B \tan r_B q_B} = \left( \frac{\kappa_B - r_B^2}{\kappa_B - p_B^2} \right)^2 \quad (34)$$

which is the same as (29) by replacing  $A$  by  $B$

### (b) Uniaxial state

For the uniaxial stress state, the solution can be obtained by replacing  $\kappa_A = 1$  and  $\kappa_B = 1$ , and is coincident with that of Steif (1986b).

### 3.4. Parabolic regime in $A$ , elliptic in $B$

Finally, consider the case where  $A$  is in the parabolic regime (only two real roots) and  $B$  remains elliptic. For this case:

$$R_A < S_A \quad (35)$$

and the elliptic relations given by (12a) hold in  $B$ . The function  $f_A$  is now written as:

$$f_A(x_2) = c_1 \sin \frac{2\pi}{\lambda} p_A(x_2 - a) + c_2 \sinh \frac{2\pi}{\lambda} r_A(x_2 - a) \quad (36)$$

where

$$\begin{aligned}
 p_A^2 &= \frac{-(R_A - 1) + \sqrt{S_A^2 - 2R_A + 1}}{S_A - R_A} > 0 \\
 r_A^2 &= \frac{(R_A - 1) + \sqrt{S_A^2 - 2R_A + 1}}{S_A - R_A} > 0
 \end{aligned} \tag{37}$$

It is interesting to note that eqn (36) for the parabolic regime in  $A$  can be reduced to the hyperbolic one by replacing  $r_A$  by  $ir_A$  (where  $i = \sqrt{-1}$ ) in (25) and making use of the identity  $\sin(ix) = i \sinh(x)$ ,  $x \in \mathfrak{R}$ . Therefore, we can obtain the bifurcation equation for this case directly from (27) as:

$$\begin{aligned}
 (R_A - S_A)^2 &[(\kappa - p_A^2)^2 V_r^A Q_p^A - (\kappa + r_A^2)^2 W_r^A G_r^A][r_B s_p^B - p_B s_r^B] - 2\zeta(R_A - S_A)(R_B - S_B) \\
 &\times \{[(\kappa - p_A^2) V_r^A Q_p^A - (\kappa + r_A^2) W_r^A G_r^A][r_B(1 + X_B) s_p^B + p_B(X_B - 1) s_r^B] \\
 &- p_B r_B (p_A^2 + r_A^2)[W_r^A V_r^A (c_r^B - c_p^B) + X_B G_r^A Q_p^A (c_r^B + c_p^B)]\} \\
 &+ 2\zeta^2 (R_B - S_B)[V_r^A Q_p^A - W_r^A G_r^A]\{r_B[(1 - S_B) X_B - S_B'] s_p^B \\
 &+ p_B[(1 - S_B) X_B + S_B'] s_r^B\} = 0
 \end{aligned} \tag{38}$$

where

$$V_r^A = r_A \cosh r_A q_A, \quad G_r^A = \sinh r_A q_A. \tag{39}$$

#### 3.4.1. Particular cases. (a) Monomaterial case

If  $\zeta \rightarrow 0$  (only  $A$ ), (38) reduces to:

$$\frac{r_A \tan p_A q_A}{p_A \tanh r_A q_A} = \left( \frac{\kappa_A + r_A^2}{\kappa_A - p_A^2} \right)^2 \tag{40}$$

which coincides with that deduced by Hill and Hutchinson (1975). This solution could also be obtained from (29) by replacing  $r_A$  by  $ir_A$ .

On the other hand, if  $\zeta \rightarrow \infty$  (only  $B$ ), solution (23) is attained.

#### (b) Uniaxial state

We could also obtain the solution for the uniaxial case, by setting  $\kappa = 1$  (for  $A$ ) and  $S' = S'' = S$  (for  $B$ ) in (38). This instance is not considered by Steif (1986b).

## 4. RESULTS

In this section, the results obtained for the bifurcation strain as a function of different geometric and material parameters are presented. The material is assumed to obey a constitutive equation in the form

$$\bar{\sigma} = \bar{\sigma}(\bar{\epsilon}) \tag{41}$$

where  $\bar{\sigma}$  and  $\bar{\epsilon}$  are the equivalent stress and strain, respectively. Three constitutive models have been considered in the calculations:

$$(i) \text{ Voce model: } \bar{\sigma} = C(1 - me^{-n\bar{\epsilon}}) \tag{42}$$

$$(ii) \text{ Hollomon model: } \bar{\sigma} = k\bar{\epsilon}^n \tag{43}$$

$$(iii) \text{ Prager model: } \bar{\sigma} = C \tanh(n\bar{\epsilon}) \tag{44}$$

where  $C$ ,  $k$ ,  $m$ ,  $n$  are constants.

Table 1. Constants in the constitutive models (95% criterion)

Model	Constants	
Voce	$C = Y, m = 1$	$n = 12$
Hollomon	$k = Y$	$n = 0.04$
Prager	$C = Y$	$n = 7.3$

From several torsion tests (López-Soria, 1993), performed on steel AISI 4130, Inconel 625 and Incolloy 825, at high temperatures and strain rates (similar to those of hot metal forming), it can be concluded that:

a peak stress is reached at an equivalent strain of about 0.25.

by neglecting the small influence of softening by dynamic recovery, a perfectly plastic behaviour could be assumed beyond that peak stress.

Accordingly, constants in (42)–(44) have been selected so as to give 95% of the maximum stress,  $Y$ , at an equivalent strain of 0.25. The resulting values are included in Table 1. The stress-strain curves obtained with these constants are compared in Fig. 3. Experience confirms that although the Hollomon model provides a good approach for small strains, the other two models behave more accurately at high strains.

For a constitutive law in the form of (41), the magnitudes  $R$ ,  $S$ ,  $S'$  and  $\xi$ , defined by (9) and (18), are given by:

$$R = \frac{\mu}{2\mu^*} = \frac{\sqrt{3}}{2} \frac{\bar{\sigma} \coth(\sqrt{3}\bar{\epsilon})}{\frac{d\bar{\sigma}}{d\bar{\epsilon}}} \quad S = \frac{\sigma_1 - \sigma_2}{4\mu^*} = \frac{\sqrt{3}}{2} \frac{\bar{\sigma}}{\frac{d\bar{\sigma}}{d\bar{\epsilon}}}$$

$$S' = \frac{\sigma_1 + \sigma_2}{4\mu^*} = \frac{3}{2} \frac{\sigma_h}{\frac{d\bar{\sigma}}{d\bar{\epsilon}}} \quad \xi = \frac{\mu_B^*}{\mu_I^*} = \frac{(d\bar{\sigma}/d\bar{\epsilon})_B}{(d\bar{\sigma}/d\bar{\epsilon})_I} \quad (45)$$

where  $\sigma_h$  is the hydrostatic stress, the incremental shear moduli are defined by the relations:

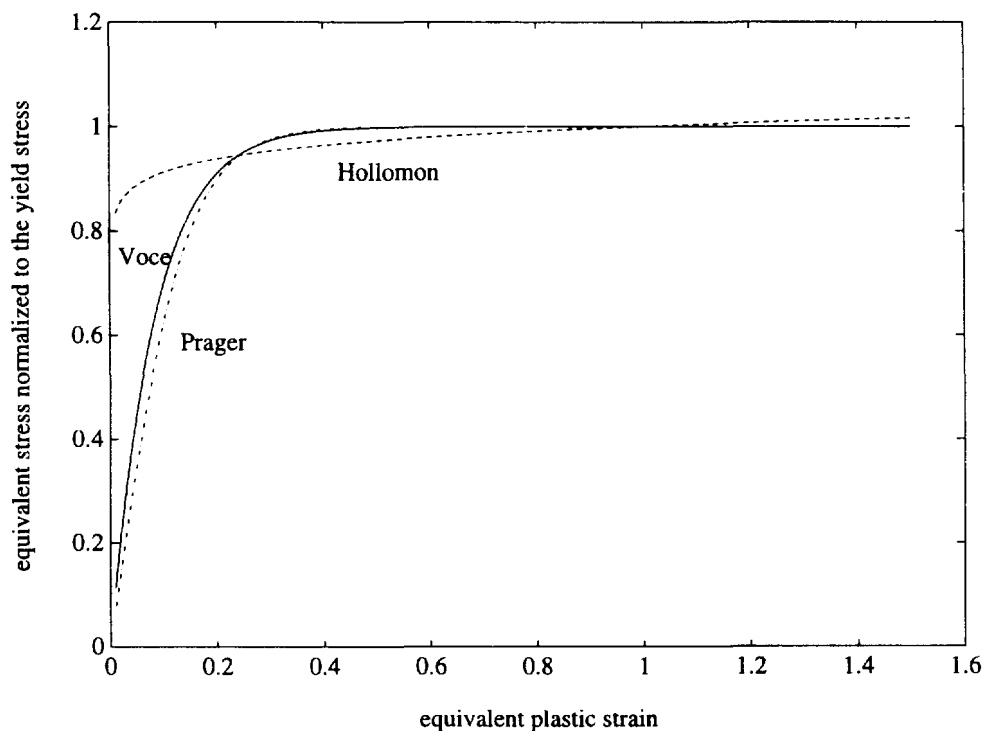


Fig. 3. Normalized equivalent stress-strain curves for the three constitutive models.

$$2\mu = (\sigma_1 - \sigma_2) \coth(\varepsilon_1 - \varepsilon_2) = (\sigma_1 - \sigma_2) \coth(2\varepsilon_1)$$

$$2\mu^* = \frac{d(\sigma_1 - \sigma_2)}{d(\varepsilon_1 - \varepsilon_2)} = \frac{1}{2} \frac{d(\sigma_1 - \sigma_2)}{d\varepsilon_1} \quad (46)$$

and the equivalent stress and strain for plane strain conditions are given by:

$$\bar{\sigma} = \sqrt{\frac{3}{2}} \sigma'_{ij} \sigma'_{ij} = \frac{\sqrt{3}}{2} (\sigma_1 - \sigma_2)$$

$$d\bar{\varepsilon} = \sqrt{\frac{2}{3}} d\varepsilon'_{ij} d\varepsilon'_{ij} = \frac{2}{\sqrt{3}} d\varepsilon_1 \quad (47)$$

The expressions for  $R$ ,  $S$ ,  $S'$  and  $\xi$  for the three constitutive models are included in Table 2.

From an inspection of (45), it can be seen that the parabolic regime is not possible for the second constitutive relation (41), because the condition  $R < S$  can never be accomplished ( $\coth x > 1, x \in \mathfrak{R}$ ). Therefore, only elliptic and hyperbolic regimes are to be considered. The limit between both regimes is defined by the conditions:  $2R - 1 = S^2$  and  $R > 1$ . This limit is shown in Table 3 for different values of the hardening exponent,  $n$ , in the constitutive laws.

The bifurcation equations presented in Section 3 can be solved numerically in terms of the wavenumber  $q_A (= 2\pi(b-a)/\lambda)$  to obtain the strain eigenvalues. For each wavenumber, a set of solutions is obtained. The critical equivalent strain will correspond to the minimum of these eigenvalues. Below this minimum, no bifurcation occurs. Calculations have been carried out for different values of the geometric and material parameters involved in the model, and for the different constitutive laws.

The range of wavelengths used in the figures has been estimated in terms of the geometric dimensions of the problem. If  $A$  denotes the amplitude of the wave and  $m$  the amplitude relative to the thickness,  $m = A/(b-a)$ , then the wavenumber can be rewritten as

$$q_A = \frac{2\pi A}{m \lambda} \quad (48)$$

For a typical relation  $A/\lambda = 0.1$  (see Gao, 1991) and assuming that the amplitude  $A$  varies between 10 and 20% of the thickness  $b-a$  ( $m = 0.1-0.2$ ), the wavenumber  $q_A$  should vary between 3 and 6.

Table 2. Expressions of the parameters in the bifurcation equation for the three constitutive models

Voce	$R = \frac{\sqrt{3}}{2n} \left( \frac{e^{n\bar{\varepsilon}}}{m} - 1 \right) \coth(\sqrt{3}\bar{\varepsilon})$	$S = \frac{\sqrt{3}}{2n} \left( \frac{e^{n\bar{\varepsilon}}}{m} - 1 \right)$
$\bar{\sigma} = C(1 - me^{-n\bar{\varepsilon}})$	$S' = \frac{3}{2} \frac{\sigma_b}{C m n e^{-n\bar{\varepsilon}}}$	$\xi = \frac{C_B m_B n_B}{C_A m_A n_A} e^{-n_A n_B n \bar{\varepsilon}}$
Hollomon	$R = \frac{\sqrt{3}}{2} \frac{\bar{\varepsilon}}{n} \coth(\sqrt{3}\bar{\varepsilon})$	$S = \frac{\sqrt{3}}{2} \frac{\bar{\varepsilon}}{n}$
$\bar{\sigma} = k\bar{\varepsilon}^n$	$S' = \frac{3}{2} \frac{\sigma_b}{k n \bar{\varepsilon}^{n-1}}$	$\xi = k \frac{n_B}{n_A} \bar{\varepsilon}^{n_B - n_A}$
Prager	$R = \frac{\sqrt{3}}{2} \frac{1}{2n} \sinh(2n\bar{\varepsilon}) \coth(\sqrt{3}\bar{\varepsilon})$	$S = \frac{\sqrt{3}}{2} \frac{1}{2n} \sinh(2n\bar{\varepsilon})$
$\bar{\sigma} = C \tanh(n\bar{\varepsilon})$	$S' = \frac{3}{2} \frac{\sigma_b}{C n} \cosh^2(n\bar{\varepsilon})$	$\xi = \frac{C_B n_B \cosh^2(n_A \bar{\varepsilon})}{C_A n_A \cosh^2(n_B \bar{\varepsilon})}$

Table 3. Limit strain between elliptic and hyperbolic regimes for the three types of constitutive equations and for different hardening parameters

$n$	$\sigma/Y$ at $\varepsilon = 0.25$	elliptic-hyperbolic limit
Voce equation		
4	0.63	0.595
8	0.865	0.415
12	0.95	0.33
16	0.98	0.273
Hollomon equation		
0.1	0.87	0.37
0.076	0.90	0.32
0.04	0.95	0.23
Prager equation		
5.5	0.88	0.395
5.89	0.90	0.3775
7.3	0.95	0.33

#### 4.1. Influence of the constitutive model

Figure 4 shows a comparison among the three assumed constitutive models for two typical cases: (a) a bilayer with an upper location of the harder material, a yield stress ratio  $k_r = Y_B/Y_A = 2$  and a thickness ratio  $r_c = (c-b)/(b-a) = 1.3$  (in Fig. 4a), and (b) a bilayer with a lower location of the harder material and ratios  $k_r = 1/2$  and  $r_c = 3$  (in Fig. 4b). By comparing these two cases, it can be seen that there is a wider range of elliptic regions in the case of a lower harder material. In general, the results obtained by using the Prager equation and the Voce model are in very close agreement. However, the bifurcation strain from the Hollomon model is somewhat lower than predicted by the other two.

Note that Prager and Voce equations seem to be more adequate to represent the elastic-perfectly plastic behaviour in metal forming at high temperature, in the sight of their asymptotic trend at high strains (see Fig. 3 and (42)–(44)). In the following, the Voce model will be selected to assess the influence of other parameters on the bifurcation strain.

#### 4.2. Influence of the geometric and material parameters

The results of Section 3 together with the Voce constitutive model will be applied in this section to elucidate the influence of a number of geometric and material parameters on the critical bifurcation strain. The following parameters are considered:

- the yield stress ratio  $k_r = Y_B/Y_A$  (for both possible locations of the harder material),
- the thickness ratio  $r_c$  (also for both locations),
- the hardening parameters  $n_a$  and  $n_b$ ,
- the hydrostatic stress parameter  $p_r$ , defined as:

$$p_r = \sigma_b/Y \quad (49)$$

Variations of the above parameters are assumed around a set of reference values given in Table 4, at the two locations of the harder material.

The influence of the yield stress ratio,  $k_r$ , is shown in Fig. 5, for the two standard cases. In the first place, it is noticed that the wavenumber that limits the elliptic regime from the hyperbolic one is different in the two cases:  $q_A = 2.5$  in Fig. 5a and  $q_A = 1$  in Fig. 5b. Therefore, there is a wider elliptic zone when the harder material is placed lower. Furthermore, below the limit wavenumber, the critical strain decreases as  $k_r$  decreases, and above it, the higher the yield stress ratio, the higher the critical strain.

Figure 6 illustrates the influence of the thickness ratio. The results for the upper location of the harder material are shown in Fig. 6a. They are very similar below  $q_A = 2$  (hyperbolic regime) for the different thickness ratios. However, above  $q_A = 2$  (elliptic regime), an increase in the strain can be noticed as the thickness ratio decreases or, equivalently, as the upper layer thickness decreases. For the lower location of the harder material, Fig. 6b shows the results. As in Figs 4 and 5, there is a more predominant elliptic region in this case. It is also noticed

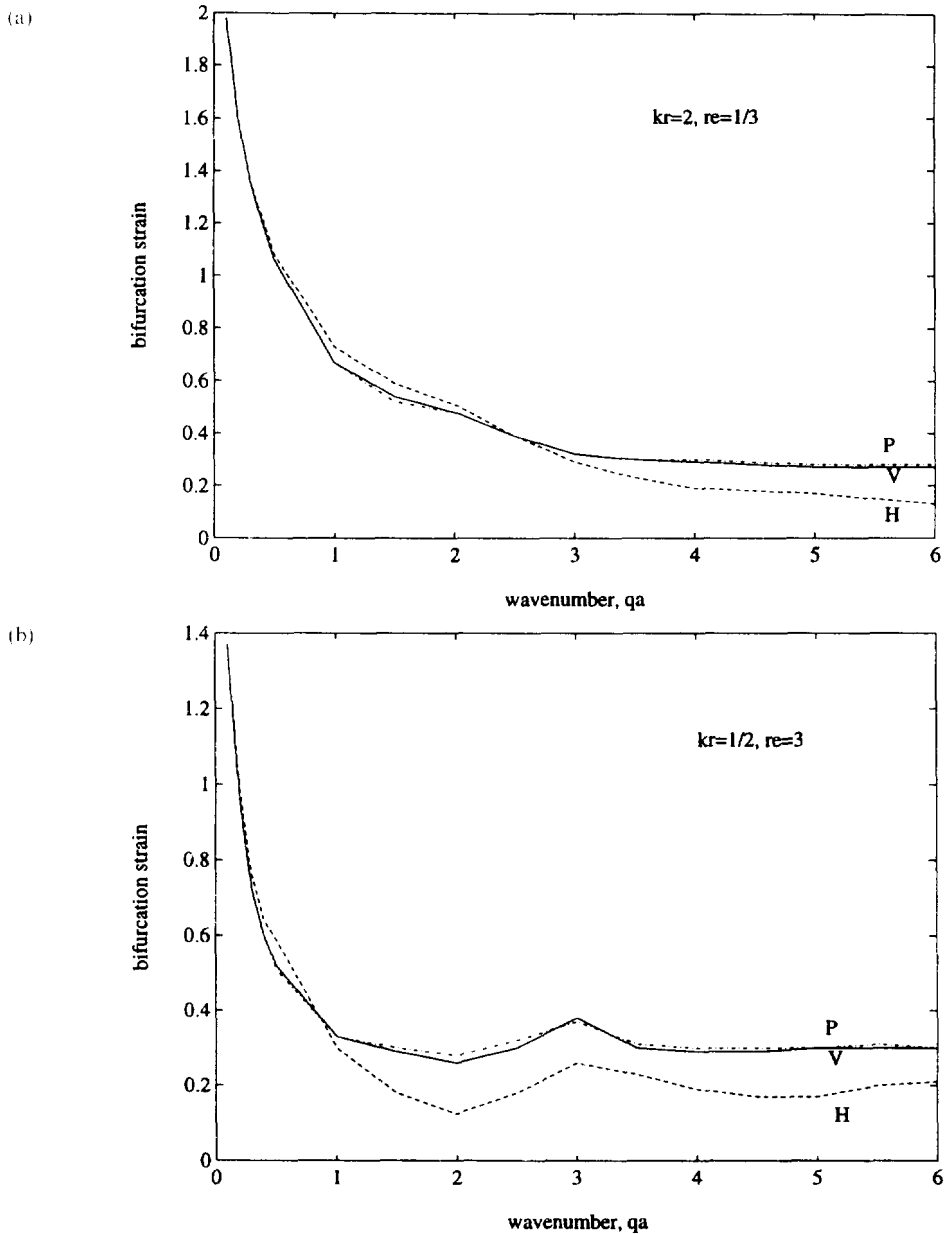


Fig. 4. Bifurcation strain for the three constitutive models, for (a)  $kr = Y_2/Y_1 = 2$ ,  $re = e_2/e_1 = 1/3$ , (b)  $kr = 0.5$ ,  $re = 3$ . ('P', 'V' and 'H' refer to the Prager, Voce and Hollomon constitutive models, respectively.)

Table 4. Reference values for the two standard cases selected

Location of the harder material	$k_1$	$r_1$	$n_1$	$n_2$	$p_1'$	$p_2'$
upper	2	1/3	12	12	1	1
lower	0.5	3	12	12	1	1

that below the limit of  $q_A = 1$  the critical strain increases on decreasing the thickness ratio. Above this wavenumber, the results are very close together, there being no appreciable difference.

Figure 7 illustrates the effect of some other parameters, attention being concentrated on the case of a lower harder material, which appears to originate to more extent spatially varying deformations, as demonstrated before. Figure 7a shows the influence of the hydrostatic stress in  $A$ , defined through the  $p_1$  parameter (see (49)). In the hyperbolic regime (below  $q_A = 1$ ), the

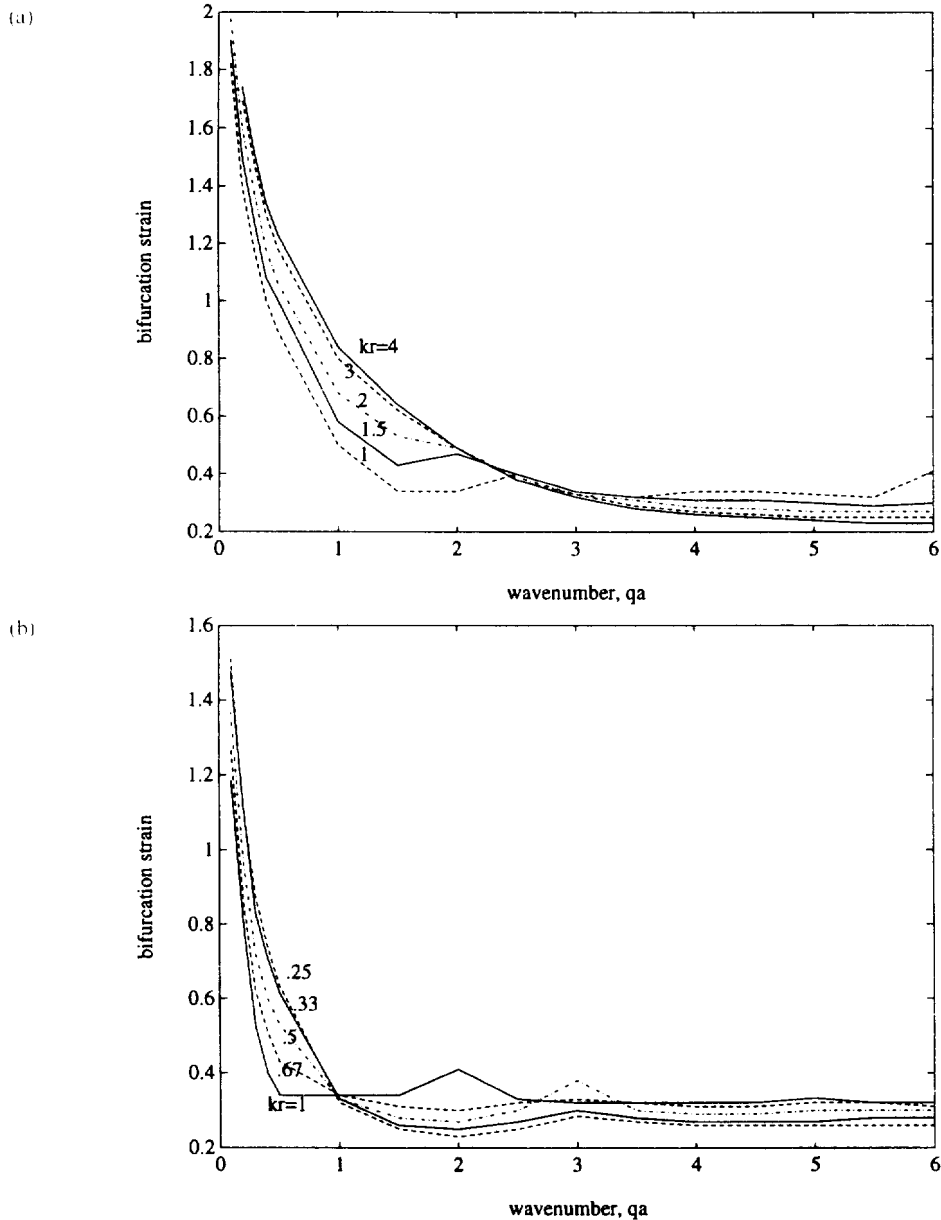


Fig. 5. Bifurcation strain for different yield stress ratios,  $kr$ , for: (a) an upper location of the harder material, (b) a lower location of the harder material.

critical strain increases as  $p_i$  increases. However, in the elliptic regime (above  $q_1 = 1$ ), the opposite trend is encountered, meaning that under a higher hydrostatic stress, bifurcation can arise at lower strains. On the other hand, the effect of varying the hardening parameter in the Voce eqn (42) is shown in Figs 7b and 7c, for  $n_a$  and  $n_b$ , respectively. It can be seen that the bifurcation strain decreases as the hardening parameter (either  $n_a$  or  $n_b$ ) increases, this indicating that instability can be promoted with a more hardening material.

## 5. DISCUSSION

The general trend of the bifurcation strains in the biaxial loading of the bimetallic layers between rigid surfaces seems similar to that observed by Steif (1986a,b) for a solid composed by alternating material layers under uniaxial tension, and by Tomita and Kim (1992) for the nonaxisymmetric bifurcation behaviour of bimaterial tubes subjected to uniform shrinkage at the external surface. Furthermore, the consistency of the solutions presented in Section 3 has

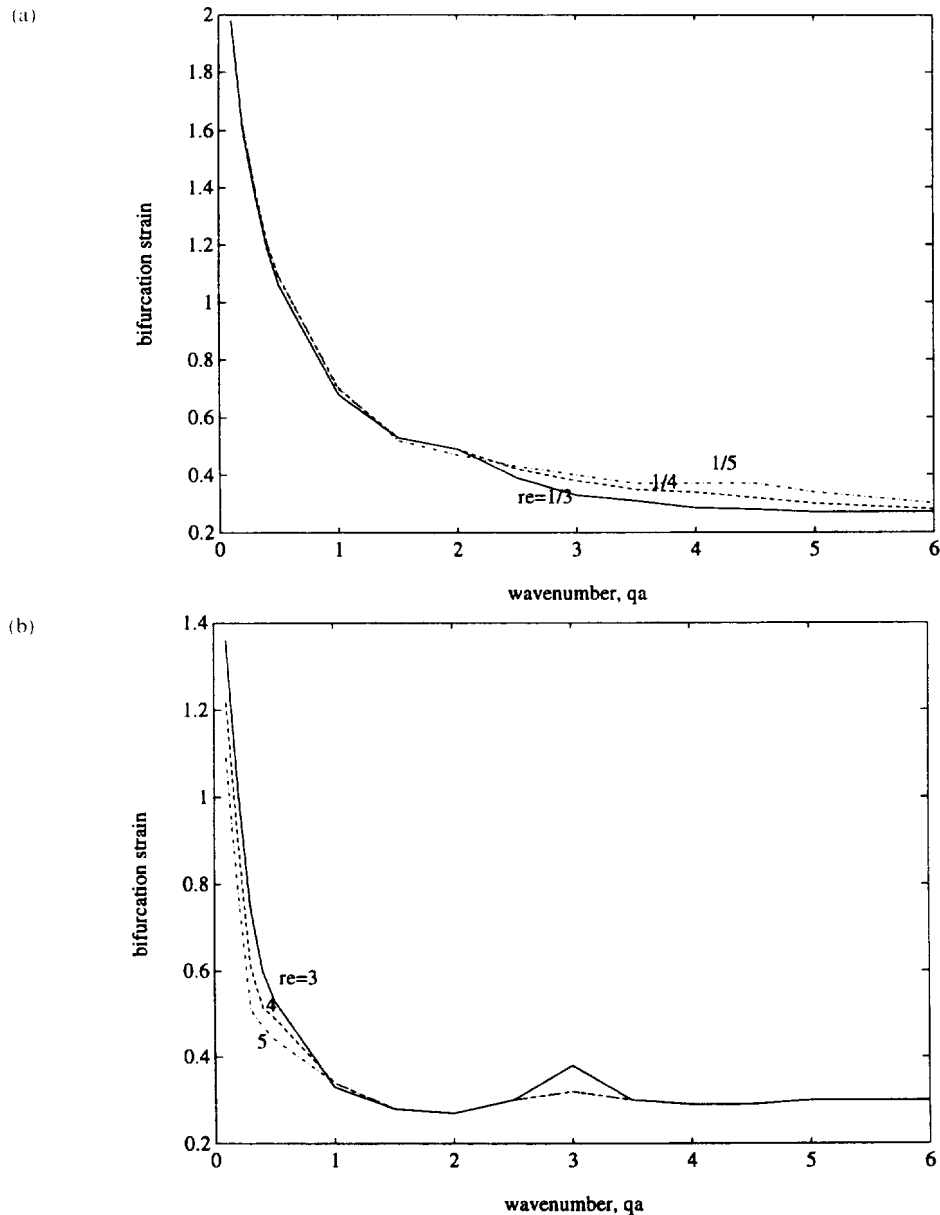


Fig. 6. Bifurcation strain for different thickness ratios,  $re$ , for: (a) an upper location of the harder material, (b) a lower location of the harder material.

been checked by calculating particular cases reported in Hill and Hutchinson (1975) and Steif (1986b).

For small wavenumbers,  $q_A$  (or, equivalently, high wavelengths,  $\lambda$ ), the critical strain increases without bounds as  $q_A \rightarrow 0$ . This behaviour was explained by Steif (1986b) as a consequence of the incompressibility kinematical restrictions and the continuity of displacements at the interface.

As the wavenumber increases, the critical strain decreases to a minimum, then exhibits some oscillations and finally tends to an asymptotic value. The minimum is more pronounced with the Hollomon model than with the Voce or Prager models. The effects of the geometric and material parameters of the problem on the critical bifurcation strain have also been analysed. They are discussed below.

The behaviour of the yield stress ratio seems in accordance with that of Steif (1986a). The increase in the yield stress ratio gives rise to a larger number of elliptic sections in the bifurcation graphs and a lower minimum bifurcation strain. The same conclusion arises from the results of Tomita and Kim (1992).

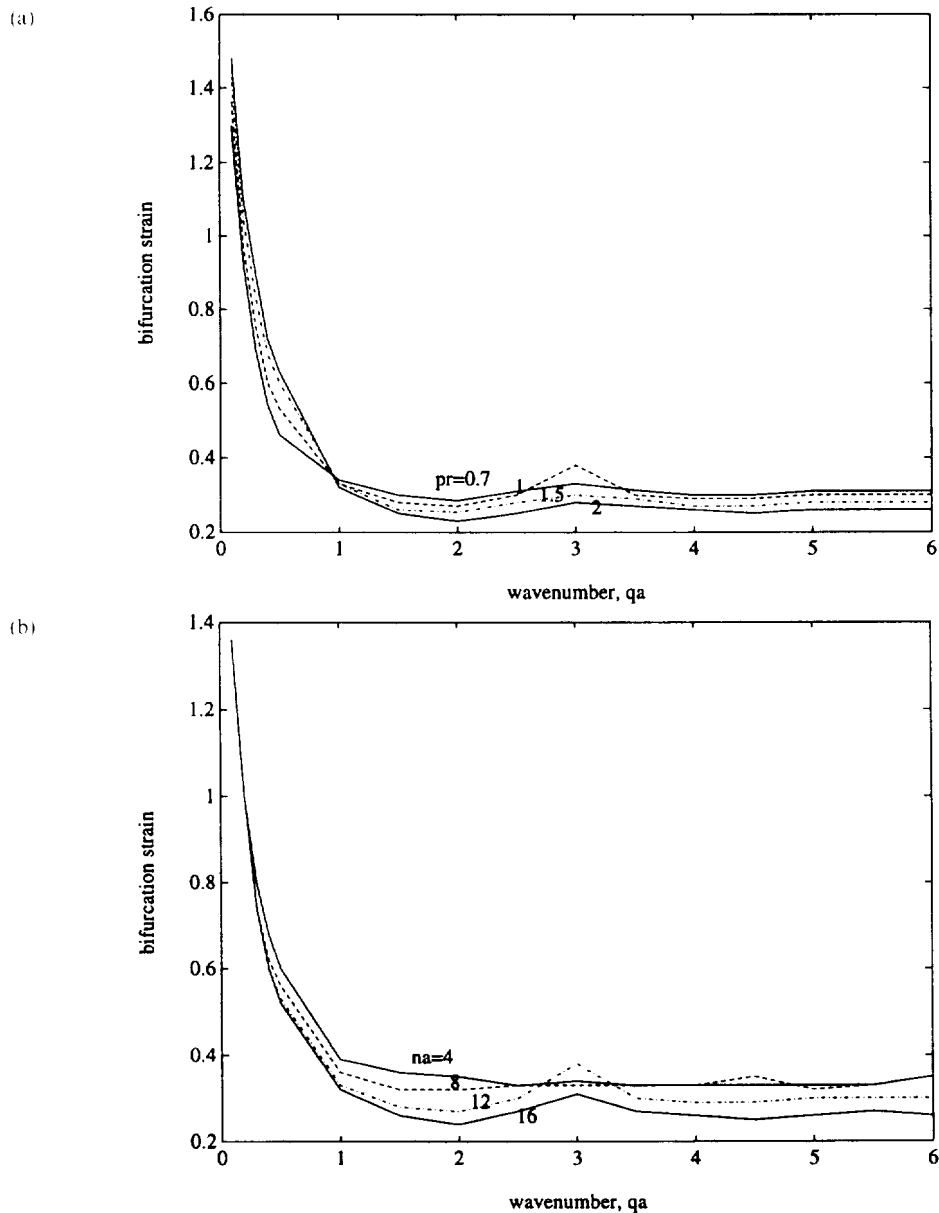


Fig. 7. Influence on the bifurcation strain, in the case of a lower harder layer, of the following parameters: (a) the hydrostatic stress,  $pr$ , in *A*, (b) the hardening parameter  $na$ , (c) the hardening parameter  $nb$ . (Continued overleaf.)

The effect of the thickness ratio, only relevant when the harder layer is placed in the upper side, can be explained by noting that the effective stress increases as it does the proportion of harder material.

On the other hand, the impact of the hardening parameter is reasonable if we bear in mind that no material instabilities occur for a rigid-perfectly plastic material (Hill and Hutchinson, 1975). This behaviour can also be verified from the results presented by Steif (1986a) and Hill and Hutchinson (1975), where it is concluded that there are more elliptic (unstable) sections on increasing the hardening rate.

Although the hydrostatic stress does not appear in the governing equations of the problem, it does affect the boundary conditions and, therefore, the final bifurcation equation. In general, an increase in the hydrostatic stress means that the stresses become more compressive.

About the influence of the constitutive model on the bifurcation graphs, the lower strains obtained with the Hollomon equation (a non-asymptotic model) can be justified by

(c)

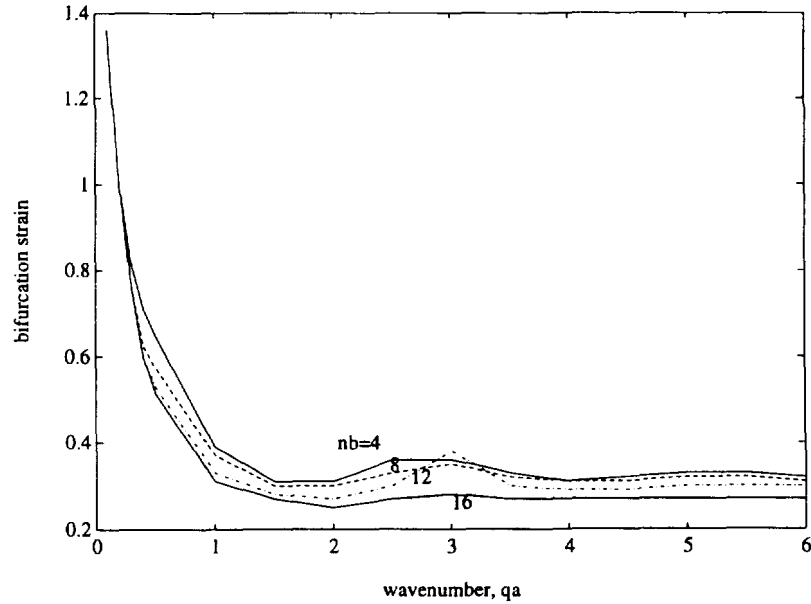


Fig 7. (Continued.)

taking into account the above comments on the influence of the hardening parameter, since a Hollomon-type model implies a more hardening material.

Finally, it is illustrative to analyse the results in some especial cases: isotropic conditions, on one side, and a rigid-perfectly plastic model, on the other.

For the isotropic case,  $R = 1/2$  and the resultant bifurcation strains in the elliptic regime, obtained from (19), are approximately constant in all the wavelength range. Therefore, it is verified that the wavenumber does not affect bifurcation for an isotropic and isothermal behaviour, in agreement with Dudzinski and Molinari (1991). In this case, as  $0 = 2R - 1 < S^2$ , only the elliptic and parabolic regimes are possible. But, as deduced by Alcaraz (1993), the critical bifurcation strain appears to be equal to the strain limit between the two regimes. This result agrees with the statement by Hill and Hutchinson (1975), that the isotropic behaviour leads to critical strains (that are accumulation points) in the limit between the two regimes.

In the case of a rigid-perfectly plastic model,  $\mu \rightarrow \infty$  and  $R \rightarrow \infty$  (see (1) and (9)) and, from eqn (20d),  $p_i = \pm 1$ ,  $r_i = 0$ . If the bifurcation eqn (19) for two elliptic regimes is divided by  $(R_i - S_i)(R_B - S_B)$ , it can be obtained that there are only two non-vanishing terms, which reduce to

$$\cos [2(q_A + q_B)] = 1. \quad (50)$$

Equation (50) means that  $q_A + q_B = n\pi$ ,  $n \in Z$ . Consequently, given the thickness ratio (or, equivalently, the ratio  $q_A/q_B$ ), there will be a bifurcation strain only for certain values of the wavelength.

## 6. CONCLUSIONS

The bifurcation analysis under biaxial loading applied to bilayered sheets between rigid surfaces has provided interesting results about the repercussion on stability of the several geometric and material parameters involved in the problem.

Firstly, an increase in the yield stress ratio between the two materials propitiates the onset of interfacial undulations. This behaviour appears for both locations of the harder material. Moreover, the case with a lower harder material results in a more unstable behaviour compared with the opposite case.

On the other hand, the effect of the thickness ratio between the two materials is only relevant when the harder layer is placed in the upper side. In this case, the bifurcation strain decreases on increasing the thickness of the upper layer.

The hardening parameter also affects the bifurcation strain. An increase in the hardening parameter of either material promotes the onset of undulations.

The influence of the applied hydrostatic stress in each material is also analysed. The higher the hydrostatic stress in either material, the more instabilities can arise at the interface.

Finally, three constitutive models (Prager, Voce and Hollomon) are considered in the analysis. It is shown that Prager and Voce equations (both asymptotic to the yield stress) lead to similar results, while the Hollomon equation (a non-asymptotic model) provides clearly lower strains.

*Acknowledgements* – One of the authors (J.L.A.) gratefully acknowledges support from the research funds of the Spanish Ministerio de Educación y Ciencia.

#### REFERENCES

- Alcaraz, J. L. (1993). Análisis de la deformación compatible y condiciones críticas de fallo en la extrusión de tubos bimetalicos. (Analysis of sound deformation and critical failure conditions in the extrusion of bimetallic tubes.) Doctoral thesis. Faculty of Engineering, University of Navarre, Spain.
- Biot, M. A. (1965). *Mechanics of incremental deformation*, Ed. Wiley, New York.
- Dudzinski, D. and Molinari, A. (1991). Perturbation analysis of thermoviscoplastic instabilities in biaxial loading. *Int. J. Solids Struct.* **27**, 601–628.
- Gao, H. (1991). A boundary perturbation analysis for elastic inclusions and interfaces. *Int. J. Solids Struct.* **28**, 703–725.
- Hill, R. and Hutchinson, J. W. (1975). Bifurcation phenomena in the plane tension test. *J. Mech. Phys. Solids* **23**, 239–264.
- Hutchinson, J. W. and Tvergaard, V. (1980). Surface instabilities on statically strained plastic solids. *Int. J. Mech. Sci.* **22**, 339–354.
- López-Soria, B. (1993). Conformado en caliente de productos bimetalicos. Caracterización microestructural de la intercara de enlace y estudio de las propiedades mecánicas del producto bimetalico. (Hot forming of bimaterial products. Microstructure characterization of the bonding interface and study of the mechanical properties of the bimaterial products.) Doctoral thesis. Faculty of Physics, University of Navarre, Spain.
- Steif, P. S. (1986a). Bimaterial interface instabilities in plastic solids. *Int. J. Solids Struct.* **22**, 195–207.
- Steif, P. S. (1986b). Periodic necking instabilities in layered plastic composites. *Int. J. Solids Struct.* **22**, 1571–1578.
- Suo, Z., Ortiz, M. and Needleman, A. (1992). Stability of solids with interfaces. *J. Mech. Phys. Solids* **40**, 613–640.
- Tomita, Y. and Kim, Y. (1992). Bifurcation behaviour of bilayered tubes subjected to uniform shrinkage under plane strain condition. *Int. J. Solids Struct.* **29**, 2723–2733.
- Young, J. B. (1976). Bifurcation phenomena in the plane compression test. *J. Mech. Phys. Solids* **24**, 77–91.

#### APPENDIX A

*Deduction of the governing derivative equation under a general stress state in plane strain*

For a more general case in plane strain, the stress state at a point of the interface is given by the stress tensor:

$$\begin{bmatrix} \sigma_{11} & \sigma_{12} & 0 \\ \sigma_{12} & \sigma_{22} & 0 \\ 0 & 0 & \sigma_{33} \end{bmatrix} \quad (\text{A.1})$$

In order to apply the equilibrium equations, we will firstly determine the time derivatives of the nominal stresses. These derivatives are related to Jaumann derivatives and true stresses through (2). By expanding this expression in the general plane case, the following relations can be obtained for the in-plane stresses:

$$\begin{aligned} \dot{n}_{11} &= \dot{\sigma}_{11} - \sigma_{12} \frac{\dot{\epsilon}_2}{\epsilon_1} - \sigma_{11} \frac{\dot{\epsilon}_1}{\epsilon_1} \\ \dot{n}_{22} &= \dot{\sigma}_{22} - \sigma_{12} \frac{\dot{\epsilon}_1}{\epsilon_2} - \sigma_{22} \frac{\dot{\epsilon}_2}{\epsilon_2} \\ \dot{n}_{12} &= \dot{\sigma}_{12} - \frac{1}{2} \frac{\dot{\epsilon}_1}{\epsilon_2} (\sigma_{11} + \sigma_{22}) + \frac{1}{2} \frac{\dot{\epsilon}_2}{\epsilon_1} (\sigma_{11} - \sigma_{22}) - \sigma_{12} \frac{\dot{\epsilon}_1}{\epsilon_1} \end{aligned}$$

$$\dot{n}_{21} = \dot{\sigma}_{21} - \frac{1}{2} \frac{\partial \dot{r}_2}{\partial X_1} (\sigma_{11} + \sigma_{22}) - \frac{1}{2} \frac{\partial \dot{r}_1}{\partial X_2} (\sigma_{11} - \sigma_{22}) - \sigma_{12} \frac{\partial \dot{r}_2}{\partial X_2}. \quad (\text{A.2})$$

Using (1) and (A.2), and introducing the flow function  $\psi$ , the following expressions are attained:

$$\begin{aligned} \dot{n}_{11} - \dot{n}_{22} &= 4\mu^* \psi_{,12} + \sigma_{12} (\psi_{,11} + \psi_{,22}) - \sigma_{11} \psi_{,12} - \sigma_{22} \psi_{,12} \\ \dot{n}_{12} &= \mu (\psi_{,22} - \psi_{,11}) - \frac{1}{2} \psi_{,22} (\sigma_{11} + \sigma_{22}) - \frac{1}{2} \psi_{,11} (\sigma_{11} - \sigma_{22}) - \sigma_{12} \psi_{,12} \\ \dot{n}_{21} &= \mu (\psi_{,22} - \psi_{,11}) + \frac{1}{2} \psi_{,11} (\sigma_{11} - \sigma_{22}) - \frac{1}{2} \psi_{,22} (\sigma_{11} + \sigma_{22}) + \sigma_{12} \psi_{,12}. \end{aligned} \quad (\text{A.3})$$

The internal equilibrium equations  $\dot{n}_{i,i} = 0$  lead to:

$$\frac{\partial^2}{\partial X_1 \partial X_2} (\dot{n}_{11} - \dot{n}_{22}) + \frac{\partial^2}{\partial X_2^2} \dot{n}_{21} - \frac{\partial^2}{\partial X_1^2} \dot{n}_{12} = 0. \quad (\text{A.4})$$

Substituting (A.3) in (A.4), the following partial derivative equation can be obtained:

$$\begin{aligned} (4\mu^* - 2\mu) \psi_{,1222} - 2\sigma_{12} (\psi_{,2222} + \psi_{,1122}) + [\mu + \frac{1}{2}(\sigma_{11} - \sigma_{22})] \psi_{,1111} + [\mu - \frac{1}{2}(\sigma_{11} - \sigma_{22})] \psi_{,2222} \\ + (\sigma_{1222} + \sigma_{1111} - \sigma_{2211}) \psi_{,1111} + 3\sigma_{12,11} \psi_{,1112} + 3\sigma_{12,22} \psi_{,1122} + (\sigma_{12,11} - \sigma_{11,12} + \sigma_{22,22}) \psi_{,2222} \\ + \left( \sigma_{12,12} + \frac{\sigma_{11,22} + \sigma_{22,22}}{2} + \frac{\sigma_{11,11} - \sigma_{22,11}}{2} \right) \psi_{,11} + \left( \sigma_{12,12} + \frac{\sigma_{22,11} + \sigma_{11,11}}{2} - \frac{\sigma_{11,22} - \sigma_{22,22}}{2} \right) \psi_{,22} \\ + (\sigma_{12,22} + \sigma_{12,11} - \sigma_{11,12} - \sigma_{22,12}) \psi_{,12} = 0. \end{aligned} \quad (\text{A.5})$$

On the other hand, the continuity conditions at the interface will be applied to  $\dot{n}_{22,1}$  and  $\dot{n}_{21}$ , which are defined by:

$$\begin{aligned} \dot{n}_{22,1} &= \psi_{,112} [\mu + \frac{1}{2}(\sigma_{11} - \sigma_{22}) - 4\mu^*] + \psi_{,222} [-\mu + \frac{1}{2}(\sigma_{11} - \sigma_{22})] + \psi_{,122} (-2\sigma_{12}) \\ &\quad + \psi_{,111} (-\sigma_{12}) + \psi_{,11} \left[ -\frac{\sigma_{11,22} + \sigma_{22,22}}{2} - \sigma_{12,11} \right] + \psi_{,22} \left[ \frac{\sigma_{11,22} - \sigma_{22,22}}{2} - \sigma_{12,11} \right] + \psi_{,12} (-\sigma_{12,22} + \sigma_{11,11} + \sigma_{22,11}) \\ \dot{n}_{21} &= \psi_{,11} \left[ -\mu + \frac{\sigma_{11} + \sigma_{22}}{2} \right] + \psi_{,22} \left[ \mu - \frac{\sigma_{11} - \sigma_{22}}{2} \right] + \psi_{,12} (\sigma_{12}). \end{aligned} \quad (\text{A.6})$$

The function  $\psi$  can be expressed as:

$$\psi = \Re \left[ \exp \left( \frac{2\pi}{\lambda} \alpha X_2 \right) \left( h_1 \sin \frac{2\pi}{\lambda} X_1 + h_2 \cos \frac{2\pi}{\lambda} X_1 \right) \right] = \Re(\tilde{\psi}) \quad (\text{A.7})$$

where  $\alpha$ ,  $h_1$ ,  $h_2$  are complex (in general), and  $\Re(\alpha) < 0$ .

Then, (A.5) turns into:

$$\begin{aligned} -(4\mu^* - 2\mu) \Re(\alpha^2 \tilde{\psi}) \omega^4 + 2\sigma_{12} \omega^4 \Re[(\alpha^2 - \alpha) \tilde{\psi}_1] + [\mu + \frac{1}{2}(\sigma_{11} - \sigma_{22})] \psi \omega^4 + [\mu - \frac{1}{2}(\sigma_{11} - \sigma_{22})] \Re(\alpha^4 \tilde{\psi}) \omega^4 \\ - (\sigma_{12,22} + \sigma_{11,11} - \sigma_{22,11}) \omega^4 \Re(\tilde{\psi}_1) - 3\sigma_{12,11} \omega^4 \Re(\alpha \tilde{\psi}) + 3\sigma_{12,22} \omega^4 \Re(\alpha^2 \tilde{\psi}) + (\sigma_{12,11} - \sigma_{11,12} + \sigma_{22,22}) \omega^4 \Re(\alpha^3 \tilde{\psi}) \\ - \left( \sigma_{12,12} + \frac{\sigma_{11,22} + \sigma_{22,22}}{2} + \frac{\sigma_{11,11} - \sigma_{22,11}}{2} \right) \psi \omega^2 - \left( \sigma_{12,12} + \frac{\sigma_{22,11} + \sigma_{11,11}}{2} - \frac{\sigma_{11,22} - \sigma_{22,22}}{2} \right) \Re(\alpha^2 \tilde{\psi}) \omega^2 \\ - (\sigma_{12,22} - \sigma_{12,11} - \sigma_{11,12} - \sigma_{22,12}) \omega^2 \Re(\alpha \tilde{\psi}_1) = 0 \end{aligned} \quad (\text{A.8})$$

where

$$\begin{aligned} \omega &= \frac{2\pi}{\lambda} \\ \tilde{\psi}_1 &= \exp(\omega \alpha X_2) (h_1 \cos \omega X_1 - h_2 \sin \omega X_1) \end{aligned} \quad (\text{A.9})$$

Equation (A.8) appears as the most general governing equation for the present plane strain problem. If we now make the assumptions that the stresses in each material are constant, and that there are no shear stresses (i.e., principal directions are assumed coincident with the coordinate axes in both materials), then (A.8) reduces to

$$(4\mu^* - 2\mu) \Re(\alpha^2 \tilde{\psi}) - [\mu + \frac{1}{2}(\sigma_{11} - \sigma_{22})] \Re(\tilde{\psi}) - [\mu - \frac{1}{2}(\sigma_{11} - \sigma_{22})] \Re(\alpha^4 \tilde{\psi}) = 0 \quad (\text{A.10})$$

which is equivalent to (3).

## APPENDIX B

*Characteristics in the bifurcation problem*

The characteristic planes of the partial derivative eqn (8) are the planes through which there can be a jump in the fourth derivatives of  $\psi$ . These planes can be obtained by imposing the vanishing of the determinant :

$$\begin{vmatrix} dx_1 & dx_2 & 0 & 0 & 0 \\ 0 & dx_1 & dx_2 & 0 & 0 \\ 0 & 0 & dx_1 & dx_2 & 0 \\ 0 & 0 & 0 & dx_1 & dx_2 \\ R+S & 0 & 2(1-R) & 0 & R-S \end{vmatrix} = 0 \quad (\text{B.1})$$

corresponding to the system of equations :

$$\begin{aligned} d\Psi_{,111} &= \Psi_{,1111}dx_1 + \Psi_{,1112}dx_2 \\ d\Psi_{,112} &= \Psi_{,1112}dx_1 + \Psi_{,1122}dx_2 \\ d\Psi_{,122} &= \Psi_{,1122}dx_1 + \Psi_{,1222}dx_2 \\ d\Psi_{,222} &= \Psi_{,1222}dx_1 + \Psi_{,2222}dx_2 \\ 0 &= (R+S)\Psi_{,1111} + 2(1-R)\Psi_{,1122} + (R-S)\Psi_{,2222} \end{aligned} \quad (\text{B.2})$$

where the last equation is (8).

Expression (B.1) provides :

$$(R-S)dx_1^4 + 2(1-R)dx_1^2dx_2^2 + (R-S)dx_2^4 = 0 \quad (\text{B.3})$$

which is the characteristic equation of (8). Therefore, if  $z_i = dx_2/dx_1$  ( $i = 1$  to  $4$ ) denotes the roots of (B.3), the characteristic planes are

$$c_1x_1 + c_2x_2 = \text{const.} \quad (\text{B.4})$$

obtained by simple integration. Real characteristic planes are only possible when (B.3) provides real  $z_i$ , and this occurs in the hyperbolic and parabolic regimes.

If we consider

$$\psi = F(c_1x_1 + c_2x_2), \quad (\text{B.5})$$

and apply  $v_1 = \psi_{,2}$ ,  $v_2 = -\psi_{,1}$ , a velocity parallel to the planes (B.4) and constant on them is obtained. For this reason, (B.4) is said to represent a local shear field. It is also found that inside a band between two parallel characteristic planes, an incremental deformation of the type (B.4) is compatible with zero nominal traction velocity (i.e., constant loading).

Consequently, the loss of ellipticity of (8) implies the possibility of strain discontinuities in the solid in the form of shear bands.